nature astronomy

Article

https://doi.org/10.1038/s41550-024-02432-3

Identification of more than 40 gravitationally magnified stars in a galaxy at redshift 0.725

Received: 11 April 2024

Accepted: 1 November 2024

Published online: 06 January 2025

Check for updates

A list of authors and their affiliations appears at the end of the paper

Strong gravitational magnification enables the detection of faint background sources and allows researchers to resolve their internal structures and even identify individual stars in distant galaxies. Highly magnified individual stars are useful in various applications, including studies of stellar populations in distant galaxies and constraining dark matter structures in the lensing plane. However, these applications have been hampered by the small number of individual stars observed, as typically one or a few stars are identified from each distant galaxy. Here, we report the discovery of more than 40 microlensed stars in a single galaxy behind Abell 370 at redshift of 0.725 (dubbed 'the Dragon arc') when the Universe was half of its current age, using James Webb Space Telescope observations with the time-domain technique. These events were found near the expected lensing critical curves, suggesting that these are magnified stars that appear as transients from intracluster stellar microlenses. Through multi-wavelength photometry, we constrained their stellar types and found that many of them are consistent with red giants or supergiants magnified by factors of hundreds. This finding reveals a high occurrence of microlensing events in the Dragon arc and demonstrates that time-domain observations by the James Webb Space Telescope could lead to the possibility of conducting statistical studies of high-redshift stars.

The high magnification afforded by massive galaxy clusters accompanied with microlensing enables us to identify individual stars in distant galaxies[1,2]. Highly magnified individual stars in distant galaxies are useful for a wide range of applications in several astronomy fields, including setting constraints on compact dark matter[3–6] and self-gravitating microstructures[7], measuring the abundance of dark matter subhaloes[8–11], setting direct constraints on the stellar populations and initial mass function of distant galaxies[2,12], and making direct observations of population III stars[13–15]. To provide meaningful constraints, these applications require a statistically sufficient, large number of distant stars identified from each lensing field. However, from previous observations, typically only one or a few individual stars have been identified in each galaxy[2,16–20], and applications using individual stars have been so far limited. With its superb light-collecting power and excellent spatial resolution, the James Webb Space Telescope (JWST) is expected to change the current situation by significantly increasing the detections of individually lensed stars from each galaxy, which would finally open up various applications of individual star detections.

Individual stars require extremely strong gravitational magnification by factors of hundreds to thousands to become bright enough to be detectable[2]. Such strong gravitational magnification is possible by a combination of strong lenses induced by massive dark matter in galaxy clusters and microlensing events by intervening compact masses, such as intracluster stars. As microlensing events are usually observed as variable sources, we typically need time-domain observations of extragalactic survey fields when searching for individual stars. Here, we report the results of serendipitously obtained JWST time-domain observations of strongly lensed galaxies.

Our target is a strongly lensed star-forming galaxy at $z = 0.725$. It is behind the galaxy cluster Abell 370, and it appears as a giant lensed arc also known as the 'Dragon arc'. Multi-wavelength images of the

e-mail: yoshinobu.fudamoto@gmail.com

https://doi.org/10.1038/s41550-024-02432-3

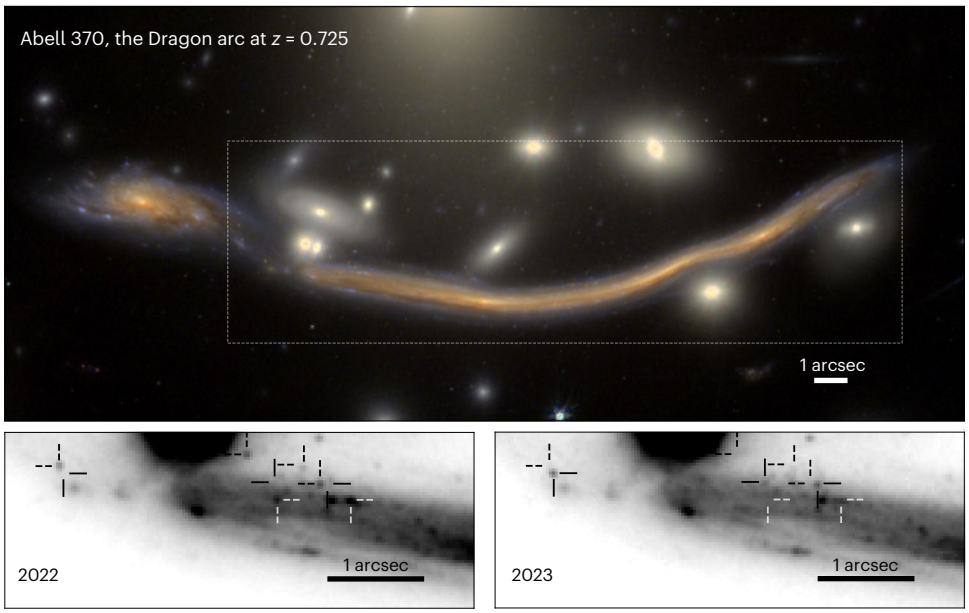

Fig. 1 | JWST observations of distant stars seen as bright transients in the Dragon arc. Upper, a false-colour image of the entire Dragon arc behind cluster Abell 370 (refs. 27,29) made using JWST filters F090W, F150W and F200W. North is up and east to the left. The dashed white rectangle shows the region of interest analysed in Fig. 2. Lower, enlargements of a part of the Dragon arc. Left, 2022 F200W image. Right, effective F200W image in 2023. The effective F200W image in 2023 was made using F182M and F210M images (Methods). Examples of apparently bright microlensing events are indicated. Dashed half-crosses show bright sources seen only in 2022 data, and solid half-crosses show sources seen only in 2023. There are many other microlensing events, but these are visible only in the differential image in Fig. 2. Scale bars, Reference angular scale of 1".

Dragon arc were captured by the near-infrared camera (NIRCam) on board JWST over two epochs: during JWST cycle 1 in December 2022 and during cycle 2 in December 2023. Both observations serendipitously used filters covering similar observing wavelength ranges within which 2 and 4.1 μm images are commonly observed. The repeat observations allowed us to perform a time-domain observation of the Dragon arc.

Using 2 and 4.1 μm images obtained across the two epochs, we searched for transient events that showed up in only one of the epochs. We used the 2 μm images as the detection images because they are deeper by ~1 mag and have a higher spatial resolution than the 4.1 μm images. The 2 μm wavelength images observed in the two epochs apparently show a large number of compact transients across the Dragon arc (bottom panels of Fig. 1). To more precisely identify fainter transients, we created a differential image by subtracting the 2 μm observation for each epoch (see Methods for more details). Thanks to the high spatial resolution and high sensitivity of each 2 μm image due to the identical position angle of the telescope, we obtained a clean differential 2 μm image, which shows many transient events that appear as bright positive and negative detections (Fig. 2). We used two complementary source-finding algorithms (DAOFIND[21] and SExtractor[22]) to efficiently detect compact and crowded transients from the 2 μm differential image (see Methods for more details). We identified 45 bright and securely detected transients with a signal-to-noise ratio of greater than 5 across the Dragon arc.

After careful investigation, we found one transient $d_{\perp} \approx 1.8$" away from the Dragon arc (event α in Fig. 2), which is probably a non-lensed transient (for example, the late stage of a supernova), where $d_{\perp}$ represents the distance from the closest position to the Dragon arc (Methods). However, simultaneously finding more than 40 supernovae from a single galaxy is improbable, even in this faint limit[23]. Also, transients seen in the 2 μm images are located around the expected positions of the critical curve within the Dragon arc. Each lens model made slightly different predictions for the positions of the critical curves due to uncertainties in the models. Thus, these transients should be strongly magnified by factors of ~10 to ~6,000, as estimated by various lensing models. As they seem to be transients typical of microlensing events, from their expected high lensing magnifications and their point source morphology in the image plane, we conclude that these transients represent microlensed stars in the Dragon arc.

To assess the basic properties of the individual lensed stars, we created a colour–magnitude diagram using photometry from differential images at 2 and 4.1 μm. We limited the sample to only F410M bright sources, namely with F410M detection at >5σ, because the F410M images are shallower than the F200W image and the ability to detect individual lensed stars was limited (Methods). With these criteria, we analysed the colour–magnitude diagram for eight microlensed stars. These stars have rest-frame F200W–F410M colours consistent with surface temperatures of ~3,000 to 4,000 K (Fig. 3)[24]. Such low surface temperatures indicate that these stars are either low-mass main-sequence stars or red giants or supergiants with an apparent luminosity of $\mu L \approx 10^{7-8}\, L_{\odot}$, where μ represents the lensing magnification factor. As these microlensing events typically have magnification factors of a few thousand, these results indicate that the F200W- and F410M-detected stars are red supergiants with intrinsic luminosities of $L_{*} \approx 10^{5}\, L_{\odot}$ and gravitationally magnified by μ factors from hundreds to a thousand.

Excluding one probable non-lensing transient, the finding of 44 microlensed stars in a single high-redshift galaxy is highly notable[2,16]. Finding many such highly magnified individual stars demonstrates the unique power of sensitive time-domain observations in near-infrared wavelengths using JWST and illustrates the high occurrence of microlensing events in the Dragon arc. Future JWST time-domain observations of the Dragon arc and other similar strongly lensed galaxies at high redshift could detect many more individual stars in galaxies at cosmological distances, which could provide us with essential information about stellar populations in high-redshift galaxies. A full analysis of the spectral energy distribution (SED) of magnified stars would be enabled by another imaging visit using the same filters. With the discovery

https://doi.org/10.1038/s41550-024-02432-3

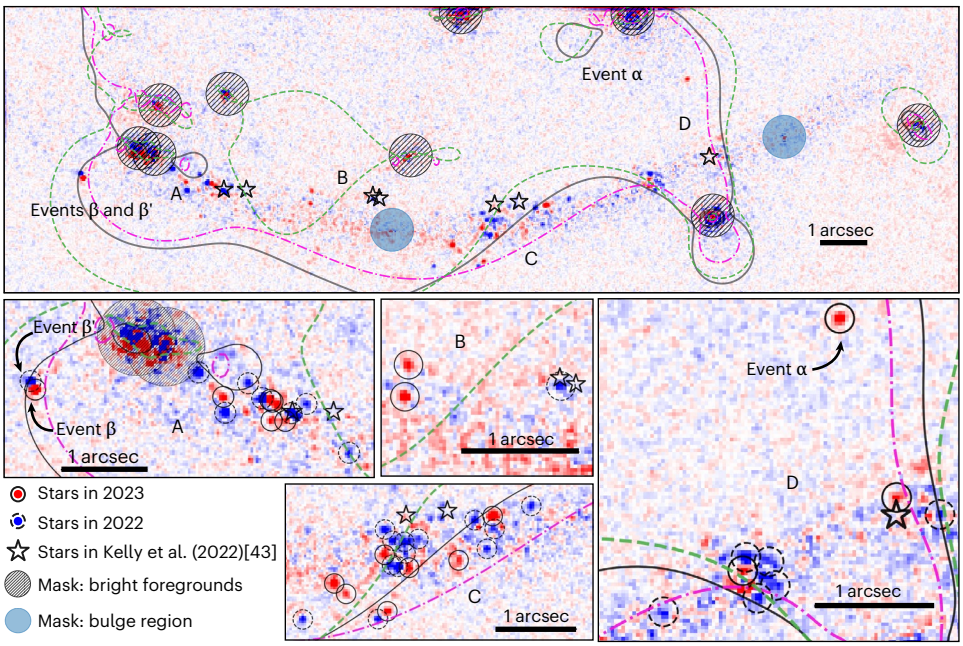

Fig. 2 | Differential images of the Dragon arc between the 2022 and 2023 epochs at 2 μm. Top, the entire differential images. Positive signals (red) show objects that appeared only in 2023, whereas negative signals (blue) show sources seen only in 2022. Contours show critical curves for $z = 0.725$ estimated from several programmes. The solid black critical curve was derived with the WSLAP+ code[63,64]. The dashed green lines were from the software lenstool[65,66]. The dashed dotted purple lines were from the light-traces-mass method[67]. Star symbols indicate the locations of previous HST detections of microlensing events[43]. Lower, enlargements of crowded transient regions indicated with **A**, **B**, **C** and **D** in the upper panel. Circles ($r = 0.12$") show detected microlensed events. Solid circles show lensed stars significantly detected in the 2023 epoch. Dashed circles indicate stars detected in the 2022 epoch. Hatched circles show the masked regions that were used to avoid contamination from bright residuals. In total, 44 microlensed stars and one probable supernova were significantly detected.

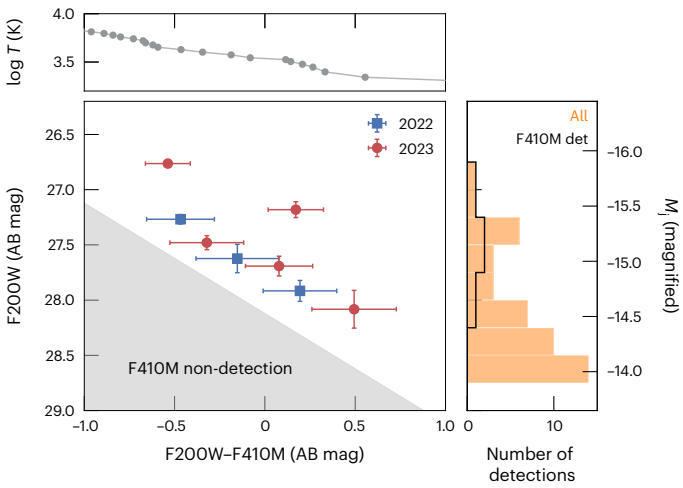

Fig. 3 | Colour–magnitude diagram of F410M-detected transients at 2 μm. Squares show events in 2022 and circles events in 2023. Except for events α and β, 0.4 mag of dust attenuation corrections were applied for all F200W–F410M colours estimated from measurements in ref. 49. Error bars represent the estimated standard deviations of the measured colours. The grey area shows the colour space inaccessible due to the sensitivity of the F410M difference image. Upper, The solid line shows typical F200W–F410M colours of giant stars with different temperatures redshifted at $z = 0.725$ (ref. 24). Right, Histogram of detected F200W magnitude and absolute magnitude in the rest-frame J band (M_J). The observed J-band absolute magnitudes of these sources show that these stars are strongly magnified by μ factors of more than about hundreds to a thousand, assuming that they are red giants or asymptotic giant stars[68]. det, detection.

of so many highly magnified individual stars, JWST has opened the possibility of conducting statistical studies of high-redshift stars and subgalactic-scale perturbations in the lensing field.

Methods

Cosmology

Throughout this paper we assume a concordance cosmology with $\Omega_m = 0.3$, $\Omega_\Lambda = 0.7$ and $h = 0.7$, for the total matter density, the cosmological constant and Hubble parameter, respectively.

Observations and reduction of JWST data

We used JWST/NIRCam imaging[25] observations from two programmes: cycle-1 GTO-1208 (the Canadian NIRISS Unbiased Cluster Survey, CANUCS, principal investigator: C. Willot[26]) and cycle-2 GO-3538 (principal investigator: E. Iani), which are publicly available. These two programmes targeted the Abell 370 cluster at $z = 0.375$ using several NIRCam filters. Observations were executed in December 2022 and December 2023, respectively, and were separated by ~1 year. The Abell 370 field includes a giant arc of a star-forming galaxy at $z = 0.725$ also known as the Dragon[27–29], which is the target of this study.

GTO-1208 CANUCS obtained images with filters F090W, F115W, F150W, F200W, F277W, F356W, F410M and F444W, each with an integration time of ~6,400 s. GO-3538 performed NIRCam wide-field slitless spectroscopy and direct imaging with filters F300M, F335M, F410M and F460M, accompanied with short-wavelength imaging using the F182M (~19,400 s) and F210M (~19,090 s) filters. Direct imaging with long-wavelength filters was also taken and had an integration time of 2,770–3,092 s.

All observations were calibrated using the standard JWST pipeline[30] v.1.11.2, with reference file jwst_1188.pmap. We also included customized routines to remove well-known artefacts, such as the subtraction of $1/f$ noise stripes in both row and column directions, template-based wisp subtraction in NIRCam short-wavelength detectors, hot-pixel masking in long-wavelength detectors and manual masking of the persistence of bright objects[25,31,32]. The astrometry of each image was carefully corrected using a combined catalogue of Hubble Space Telescope (HST) sources detected with HFF/BUFFALO

images[33] and the DESI Legacy Imaging Survey catalogue[34], both registered to Gaia[35]. As a result, each image was well aligned, with an absolute astrometric error of <0.03", and an internal r.m.s. astrometric error of ~0.004" for all >5σ sources. The final mosaicked images were drizzled with pix_frac = 1.0 and a pixel size of 0.03".

Identifications of microlensing events

Our target is a strongly lensed star-forming galaxy, the Dragon arc, at $z = 0.725$ and behind Abell 370. This highly lensed galaxy was originally known as 'the Giant Arc'[27–29]. Later, Dragon arc was labelled during one of the image releases of the HST advanced camera for surveys in 2009.

We first investigated the Dragon arc by directly comparing the F200W (2022) and F182M (2023) images. We found that several bright sources were seen in only one of the epochs. These represent potential transient events across the Dragon arc. Then, to more precisely identify fainter transient events, we subtracted a combined F182M + F210M image (2023) from the F200W image (2022). We used $\lambda_{obs} = 2$ µm images to identify transients instead of the repeated F410M filter because the 2 µm data are deeper by ~1 mag and have a higher spatial resolution. To make the 2023 epoch F182M + F210M image (the 'effective' F200W image), we first homogenized the point spread function (PSF) for the F182M and F200W images to match their PSFs to that of F210M. The PSF for each image was made using WebbPSF (ref. 36) by applying the wavefront measurements for the closest date of each observation. Convolution kernels were produced using pypher (ref. 37) by applying a regularization factor of 0.0001. The kernels were convolved using the convolve2d function of the scipy.signal submodule[38]. Using the PSF-homogenized F182M and F210M images, we created an effective F200W image by linearly interpolating fluxes at the pivot wavelength of each filter. We then verified that the effective F200W-2023 image provided fluxes consistent with the F200W-2022 image by measuring the aperture flux of bright (F200W magnitude of $m_{F200W} > 23.2$ mag) sources in both images. We found the difference between the fluxes was $0.4^{+0.6}_{-1.8}$%. The differential image was then created by subtracting the effective F200W-2023 image from the PSF-homogenized F200W-2022 image.

Finally, we subtracted the global background of the differential image, which removed any large-scale background. The systemic large-scale background was due to differences in the background subtraction (for the sky and intracluster light) during the production of mosaicked images. As a result, a clean differential image was created with a pixel distribution of ~0.0 ± 0.8 nJy. The differential image clearly shows significant positive and negative peaks across the Dragon arc, indicating a large number of transient events were observed over the two epochs (Fig. 2).

We used DAOFIND (ref. 21) incorporated in the photutils.detection submodule and SExtractor (ref. 22) to detect microlensing transients from the differential image. These two source-finding algorithms are complementary in that DAOFIND efficiently detects circular Gaussian sources in crowded regions whereas SExtractor can detect less circular sources that can also be found in the crowded regions in the differential image.

For the SExtractor run, to detect compact sources, we applied a minimum number of connected pixels of four, each of them with flux >2.5σ above the background standard deviation by setting DETECT_MINAREA = 4 and DETECT_THRESH = 2.5 (>5σ detection). To deblend crowded sources, we set the contrast parameter DEBLEND_MINCONT = 0.0005. With these settings, we ran SExtractor for positive and negative instances of the differential image, corresponding to transient events in 2023 and 2022, respectively. For the DAOFIND run, we used a 5σ threshold of 0.038 MJy sr^{-1} (0.7 nJy pix^{-1}) and a kernel full-width at half-maximum FWHM = 2.5 pixels. Similarly, DAOFIND was used for positive and negative instances of the differential image.

For both of the source detections, we masked regions close to bright sources (for example, bright cluster member galaxies and bulges of the Dragon arc) in the original F200W image. This avoided contamination from residuals caused by minor PSF differences between 2022 and 2023, which were apparent in the differential image. All masks had a fixed radius of $r = 0.45$" and were centred on the brightest pixel of each galaxy and bulge. To be conservative, the radius was manually determined using the brightest and largest residuals in the north-west and south-west parts of the differential image. Between the two epochs, the position angle varied by ~2°, and the difference in the FWHMs of the PSFs was <5%.

To assess the impact of the noise signal on detection, we ran the same source-finding routine over the same F200W differential image for several types of galaxies (for example, clumpy or smooth morphology with different luminosities). Except for genuine transients, such as supernovae that were also detected in other bands, we did not detect any significant bad pixels that appeared only in a single band with similar significance. Therefore, we conclude that the transients detected on the Dragon arc are not data-quality artefacts but real transient events.

Using the PSFphotometry routine of the photutils.psf module, we assessed the sizes of the individually detected transient events by subtracting scaled PSFs at their positions. The residuals seem to be consistent with background noise, leading us to conclude that the transients are consistent with point sources.

Was there contamination from strong emission lines?

Note that it is possible that strong emission lines from H II regions are masquerading as transients due to the imperfect match between the F182M + F210M and F200W filter transmission curves. At $z = 0.725$, He I λ1.083 µm and Paschen γ could elevate the flux density from F182M photometry and Paschen β may boost the F200W photometry, if these are strong enough. In the 'head' of the Dragon arc (the least magnified image of the Dragon arc seen in the easternmost part of Fig. 1), three bright clumps can be tentatively seen as faint F200W (2022) excess sources with peak brightness ~1 nJy pix^{-1} in the difference image. However, counter images of these clumps were not selected in our sample, as they are much fainter than our selected transients. Additionally, no underlying compact star-forming clumps were seen in the continuum emission. For these reasons, we conclude that the emission-line contamination in our transient sample is negligible.

Was there contamination from star clusters?

Note that star clusters rather than single stars might have contaminated the sample if microlenses can magnify such spatially extended objects. However, as we argue below, this is not the case, and we securely reject the possibility of contamination in our microlensed transient samples from magnified star clusters.

To achieve a microlensing magnification boost factor $\mu_? = 10$ through a solar-mass lens in the Abell 370 cluster given a macrolensing magnification of 100 (Supplementary Table 1), the maximum allowed source size is $r_? = 2\theta_E D_s/\mu_?$, where θ_E is the Einstein radius for the effective microlens and D_s is the angular diameter distance at $z_s = 0.725$ (refs. 39,40). This was found to be $r_? \approx 5.4 \times 10^3 (10/\mu_?)$ au. This distance is too small compared to the typical distance between bright stars in a star cluster that can be detectable through magnification by approximately ×1,000 due to microlensing events[41,42]. Thus, a microlens does not provide enough magnification for such a spatially extended object. This means that even if the observed supergiants reside in star clusters, the detected sources cannot be the entire star cluster. Assuming an extreme case of 1,000 very bright stars within 1 pc (ref. 41), the projected separation between them would be large (~10,000 au) and simultaneously achieving a microlensing boost for many of them would be impossible.

Photometry

To measure the F200W fluxes of the detected transients, we performed forced aperture photometry on the difference images at the detected

positions. We used fixed-aperture photometry with an aperture radius of 0.06 arcsec. The photometric errors were estimated by placing random apertures of the same size on the transient-free regions of differential images. To take into account realistic Poisson noise from the host galaxy, we placed random apertures only where the surface brightness in the F200W image was 0.4–50 nJy pix^{-1}, which is close to the surface brightness of the background in the Dragon arc around the transient positions. We performed aperture-correction based on the PSF models obtained using WebbPSF (ref. 36). The 5σ detection limit was, therefore, determined as 28.75 AB mag in the difference image.

We also performed photometry for transients using F410M images because F410M is the only repeated filter used in both epochs. However, the F410M images are shallower than the F200W images as they were observed as a part of grism observation in GO-3538. For this long-wavelength photometry, we limited our sample to only F410M bright sources, namely F410M detection only at >5σ. Because of the larger PSF and higher sky background, longer-wavelength images have only limited detection capability. In particular, within the bright region of the Dragon arc, strong, correlated noise buries weak transient signals. Additionally, the larger PSF of F410M (FWHM ≈ 0.14") prevented us from detecting transients in crowded regions where F200W-based detections have separations of ~0.1". Therefore, we focused on F410M photometry and analysis only for the brightest microlensing events (Supplementary Fig. 1). For these bright sources, we similarly performed forced aperture photometry with a fixed aperture radius of 0.1 arcsec. The F410M detection limit for a transient was ~27.7 AB mag. The much smaller number of transient detections in F410M reflects the shallowness of the F410M differential image, its larger PSF, the actual surface temperature of each individual star (Fig. 3) and differences in the dust opacity in each line of sight.

We did not perform photometry for microlensed stars using other filters in this study except for events α, β and β' (see SED analysis of bright sources). These three events appear around the region where backgrounds are smooth and, thus, easy to estimate using the surrounding area. However, for most cases, the background was part of the Dragon arc itself, leading to uncertainty in estimating the background and performing accurate photometry for each source. This was because we did not have repeated observations for all filters. A full reliable SED analysis would require another imaging visit using filters that have existing images.

Summary of transient events in 2022 and 2023

Using two independent source detections, we found 44 and 31 sources from SExtractor and DAOFIND, respectively. All sources detected by DAOFIND were also detected by SExtractor. We detected 45 transient events in the Dragon arc; 27 in the 2022 observation and 18 in the 2023 observation (Supplementary Table 1). Compared with previous identifications of microlensing events and magnified single-star observations (for example, eight in the Dragon arc identified with the HST Flashlights programme down to 3.3σ significance[43]), our finding of 44 microlensing events in a single galaxy is very notable and demonstrates the extremely high occurrence rate of microlensing events in the Dragon arc captured by JWST. This is because the Dragon arc has a lower redshift than other galaxies that host microlensing events (for example, refs. 2,20,44), and therefore, more stars were visible to the JWST when highly magnified.

Detecting microlensing events requires extremely high magnification (μ ? 10^3). Therefore, they occur frequently around the critical curves of the large-scale gravitational lenses powered by major dark matter haloes of galaxy clusters (macrolensing). The locations of our detections of microlensing events are consistent with macrolensing critical curves for $z = 0.725$ objects previously estimated in different studies and with different software and methods (Fig. 2). The estimated magnification for a macrolens based on existing cluster mass models is typically μ ? 10^2, although there are large uncertainties, as indicated by the model-to-model scatter in Supplementary Table 1.

Although the positions of the detected microlensing events are consistent with the macrolensing critical curves, note that existing lens models of the Abell 370 cluster do not simultaneously explain all the microlensing events. In particular, several transient events have large angular offsets from the expected positions of macrolensing critical curves (for example, region C in Fig. 2). These large offsets between the macrolensing critical curve and microlensing events may indicate the complex structure of the dark matter subhalo structure of the lensing cluster (for example, refs. 8,9,45) or the uncertainty in gravitational lens models. In-depth analyses of detailed mass models with complex subhalo distributions incorporating the uncertainty in lens model will be important in future works.

Furthermore, we identified an event with a large angular offset ($d_\perp \approx 1.8$" or 1.7 kpc assuming $z = 0.735$) from the Dragon arc. We call this event α (Fig. 2), and a detailed analysis and discussion are presented in Event α.

Note that many point-like residuals in the Dragon arc were not selected as transients because of our conservative 5σ detection limit (Fig. 2). These surface brightness fluctuations were probably caused by fainter microlensed events or events away from the peak phase. For fainter magnitudes, we expect that it is highly probable that several, independently microlensed stars blended within the PSF collectively contribute to the observed flux variability. Such signals have been discussed in the contexts of pixel variability[46] and the collective variability of unresolved stellar associations[39]. Future deep and higher spatial resolution multi-epoch imaging observations, such as with 30 m class telescopes with adaptive optics, may be able to resolve and identify such faint and crowded single stars.

We found that, in region A of Fig. 2, one of the spatial locations of our sample overlaps with previous transients found by HST[43]. These may represent close microlensing events or a repeated microlensing event of the same star. Although the probability of finding the same star microlensed in different epochs is very low, doing so is still possible, especially if the background object is a binary star system, as discussed for a $z \approx 6$ star[20]. Disentangling these possibilities or confirming such repeated events requires, at least, multi-wavelength observations of the events in future repeat observations using JWST. In addition, the probability of seeing several microlensing events from the same background star would be increased if a millilens was near the line of sight, as discussed in ref. 47.

Colour–magnitude diagram

The colour–magnitude diagram of the detected lensed sources shows that they have red colours in F200W–F410M > 0 mag (roughly corresponding to $J - K$ in the rest frame; Fig. 3). Previous Herschel observations at 100–500 μm have shown that the Dragon arc is a dusty star-forming galaxy[48] and that it exhibits significant interstellar dust attenuation of up to $E(B - V) = 0.4$ mag (ref. 49). This implies the need to apply colour corrections between F200W and F410M of up to 0.4 mag to derive the intrinsic F200W–F410M colours of each source, assuming a uniform dust screen. We simply applied a colour correction of 0.4 mag to classify the possible stellar types for the detected sources, except for the off-arc events α and β, but we caution that there is a potential variation of dust attenuation for the observed stars, which cannot be corrected with the data taken so far.

Sources detected in microlensing events have F200W–F410M colours of −0.5 to +0.5 mag (Fig. 3). By comparing with theoretical stellar atmosphere spectra of giant stars (lowest surface gravity available at each effective temperature in the set in ref. 24, under the assumption of [M/H] = 0), these colours are consistent with typical ranges of stellar spectra with temperatures T ? 5,000 K. Owing to their low temperature and high luminosity, these sources are red giants or supergiants (and potentially binaries) magnified by factors $\mu > 1{,}000$ and thus reach

absolute J-band magnitudes of −14 to −16 AB mag (see also SED analysis of bright sources, below). These colour distributions are particularly biased towards red sources because we detected sources with F200W filters and because of the shallowness of F410M observations. Detecting higher-temperature stars at this redshift (for example, ?8,000 K) would require multi-epoch observations at $\lambda_{obs} < 1$ μm (ref. 43).

SED analysis of bright sources

For three particularly bright events, α, β and β', we studied their SEDs using multi-wavelength photometry. As these events occurred in regions that are away from the brightest part of the arc, a more accurate background subtraction was possible using single-epoch data. We found that a full SED analysis of other transient events was difficult. This was because correctly subtracting the background from their photometry was possible only for the repeating F200W and F410M bands. For events α, β and β', using backgrounds in non-repeating bands would be possible, as their backgrounds are smooth. Nevertheless, their photometry might still be contaminated by their backgrounds. Thus, the photometry in Supplementary Table 1 is more accurate as it uses the actual background for each transient event, whereas the single-epoch data in Supplementary Table 2 is useful for full SED analyses. We conducted photometry for these events using background-subtracted images of observations in 2022 and 2023. Aperture photometry was performed with aperture radii of 0.06 arcsec and 0.10 arcsecfor short-wavelength and long-wavelength filter images, respectively. Annuli with a width of 0.10 arcsec were used to measure local backgrounds, and flux density uncertainties were measured from random aperture experiments. The photometry obtained is summarized in Supplementary Table 2.

Event α

From our analysis of the difference images between the 2022 and 2023 observations, event α has the largest angular separation from the arc (~1.8"; Fig. 2). The SED of event α is shown in the top left panel of Supplementary Fig. 2. We found that a $T = 2{,}200$ K template among the examples in the stellar spectral library in ref. 24 provides the best match to the observed SED. Therefore, if event α is a microlensing event of a single star, it would be a cool star in the galaxy halo of the Dragon arc. We also examined the F182M and F210M light curves of event α over epoch 2 (3.4 day span in the observer frame). Despite the noisy data for each telescope visit, we detected no evidence of a significant brightness change (<0.7 mag) within this time frame.

However, most of the existing cluster mass models do not explain the required high magnification of event α needed for it to be observed as a microlensing event (typical macrolens $\mu \approx 10$–100 in Supplementary Table 1). Assuming a macro- plus microlensing magnification of $\mu = 1{,}000$ at $z_s = 0.725$ and no dust extinction, event α should have an absolute J-band magnitude of −7.2 AB mag in the rest frame. Given the expected low number density of very luminous, short-living stars in galaxy haloes, the likelihood of event α being a microlensing supergiant star in the Dragon arc is low. Although one could assume a significantly stronger lensing magnification to accommodate the lower intrinsic luminosity of the source, this would require a much smaller impact parameter (and, thus, a rarer chance) for the alignment of the microlens with the background star. In addition, the separation of event α ($d_\perp \approx 1.8$") from the host galaxy is too large for an evolved star at this distance, making the interpretation of event α as a microlensing event even less probable. Therefore, we also consider the following physical explanations of event α and explore their likelihood:

- Type Ia supernova in Abell 370: Possible. Given its proximity to one cluster member galaxy of Abell 370, event α was probably a supernova at the cluster redshift. Because most galaxies in the Abell 370 cluster are quiescent and, although some cluster galaxies are known to have core-collapse supernovae (for example, refs. 50,51), we consider event α to be a probable type Ia supernova. At the cluster redshift $z = 0.375$, the observed F200W magnitude implies an absolute magnitude of −13.2 AB mag at 1.5 μm. With this brightness, it could only have been a type Ia supernova in its nebular phase, that is ~200 days post-peak in the rest frame (for example, ref. 52). Note that the two epochs of JWST observations have a separation of 260 days in the $z = 0.375$ rest frame, placing a stringent upper limit on the age of event α if it is a cluster supernova. The middle left panel of Supplementary Fig. 2 compares the SED of event α with the JWST spectrum of the nearby type Ia supernova 2021aefx at +255 days post-peak (the nebular phase[53]). We found that the observed SED of event α can be explained by this spectral template with similar reduced χ squared value of $\chi^2_{reduced}$ (1.6) reduced to that of the aforementioned cool star template ($\chi^2_{reduced} = 1.6$). The residual is then mostly dominated by the F460M non-detection. Therefore, we conclude that event α could have been a type Ia supernova at the redshift of the foreground cluster.
- Kilonova in Abell 370: Unlikely. At $z = 0.375$, the observed F200W magnitude could match that of a kilonova like AT 2017gfo (the electromagnetic counterpart of GW170817)[54] at ~10 days post-merger[55]. At this epoch, AT 2017gfo already had a red rest-frame $H - K$ colour of 1 AB mag. However, this was not observed for event α in F210M − F300M. Therefore, we conclude that event α was unlikely to have been a kilonova at the cluster redshift. However, our knowledge of the light curves and SEDs for kilonovae is still very limited, and they could show a large diversity because of different ejecta properties[56].
- Luminous red nova in Abell 370 or the Dragon arc: Unlikely. A massive star merger can trigger luminous red novae that reach an absolute V-band magnitude of approximately −15 mag (for example, ref. 57). They can also have a similar rest-frame near-infrared colour as event α. However, we argue that the likelihood of there being a massive stellar progenitor in either the halo of Dragon or Abell 370 quiescent member galaxies is considerably low.
- 'Hostless' supernova at z ? 1–2: Possible. Event α could also have been a lensed supernova hosted by a low-mass galaxy that has not been detected, even by JWST. This is known as a 'hostless' supernova. If event α was a supernova at z ? 2, based on the glafic lens model[58,59], we would expect the detection of a counter image of the supernova with a short time delay to event α (?20 days) but potentially larger magnification. If event α was a supernova at z ? 0.8, then with the large magnification ($\mu \approx 10$) and limited evolution time (<1 year in the observed frame), event α should have been as bright as ?27 AB mag at 2 μm, that is, 1 mag brighter than actually observed. Therefore, if event α was a hostless supernova, it could only have been at z ? 1–2. Using spectral templates for type Ia supernova from ref. 60 and the software SNCosmo (ref. 61), we found that the SED of event α can be explained by a type Ia supernova at $z \approx 1.32$ with $\chi^2_{reduced} = 1.7$, for which the age $t \approx +129$ days post-peak (+300 days in the observer frame; Supplementary Fig. 2, bottom left panel). At this redshift, the several images would be expected to be non-detections in the obtained JWST data, either because of large differences in their arrival times or because of their proximity to bright cluster member galaxies. Therefore, we do not rule out the possibility that event α was a hostless supernova at $z \approx 1.3$.

As a final remark, naturally, there are other transient sources (for example, tidal disruption events) that could be used to interpret event α. However, we believe that the above discussions cover most of the known possibilities, and we conclude that event α could be interpreted either as a nebular-phase type Ia supernova at the Abell 370 redshift or as a hostless supernova at $z \approx 1.3$.

Events β and β′

Events β and β' were found in the 2022 and 2023 observations, respectively, at the most south-eastern position of the Dragon arc (Fig. 2). Both events are some of the brightest among the current microlensing events found in the 2022 and 2023 images. As the locations of these events are in the outer disk region of the Dragon arc, we expected low dust attenuation for these two sources. Thus, we assumed no dust attenuation for sources observed in either event β or event β'.

The right panel of Supplementary Fig. 2 shows the observed fluxes of events β and β'. Using the spectra of stellar atmosphere models in ref. 24, we performed χ^2 minimization. We found that low-temperature stars with surface temperatures of T = 3,000 to 3,300 K fit well and a T = 3,200 K star gives the minimum $\chi^2_{\rm reduced} = 1.1$ for the SED of event β. Similarly, the observed SED of event β' is well represented with a star with surface temperature = 3,500 to 3,700 K whereas a T = 3,500 K star gives the minimum $\chi^2_{\rm reduced} = 4.7$. With these fits, we found the apparent luminosity of events β and β' to be $\mu L_{\rm bol} \approx 1 \times 10^8\, L_\odot$ and $\mu L_{\rm bol} \approx 8 \times 10^7\, L_\odot$, respectively.

Due to their low temperatures, as represented by their red colours, these events could be microlensed red giant or supergiant stars that are strongly magnified with $\mu \gtrsim 1{,}000$. The different spectral shapes of events β and β' suggest that they are different stars, rather than several images of a single star. Moreover, as low-temperature stars at high redshift are bright only in $\lambda_{\rm obs} \gtrsim 2$ μm, these sources demonstrate the importance of such near-infrared observations for building complete stellar samples at high redshift.

An alternative interpretation is that these two stars are, indeed, the same star multiply imaged as a result of an astrometric perturbation induced by dark matter subhaloes. Such events have been predicted by ref. 8 and occur specifically around the critical crossing region, such as locations near events β and β' (see also ref. 2). In this case, the differences in the observed SEDs are interpreted as being due to the intrinsic variability of the magnified star. In fact, such variability in stars accompanying changes in their surface temperature and SEDs have been observed in nearby stars such as cepheids. Although a definitive conclusion is difficult to obtain with existing photometry using single epochs, confirmations of such magnified close-paired stars in large numbers would allow us to investigate the subhalo structure of dark matter as well as to constrain dark matter physics. Future JWST time-domain observations using matched filters may allow us to obtain accurate multi-wavelength photometry for individually magnified stars and enable us to conduct such studies.

Data availability

The 2 μm differential image generated and analysed during the current study is available from https://github.com/yfudamoto/the_dragon_arc2024.git. Other datasets generated are available from the corresponding author on reasonable request. The raw data from GTO-1208 (CANUCS) are available on the Mikulski Archive for Space Telescopes at https://doi.org/10.17909/ph4n-6n76 (ref. 62).

References

1. Miralda-Escude, J. et al. The magnification of stars crossing a caustic. I. Lenses with smooth potentials. *Astrophys. J.* **379**, 94 (1991).
2. Kelly, P. L. et al. Extreme magnification of an individual star at redshift 1.5 by a galaxy-cluster lens. *Nat. Astron.* **2**, 334–342 (2018).
3. Venumadhav, T., Dai, L. & Miralda-Escudé, J. Microlensing of extremely magnified stars near caustics of galaxy clusters. *Astrophys. J.* **850**, 49 (2017).
4. Oguri, M., Diego, J. M., Kaiser, N., Kelly, P. L. & Broadhurst, T. Understanding caustic crossings in giant arcs: characteristic scales, event rates, and constraints on compact dark matter. *Phys. Rev. D* **97**, 023518 (2018).
5. Diego, J. M. et al. Dark matter under the microscope: constraining compact dark matter with caustic crossing events. *Astrophys. J.* **857**, 25 (2018).
6. Vall Müller, C. & Miralda-Escudé, J. Limits on dark matter compact objects implied by supermagnified stars in lensing clusters. Preprint at arxiv.org/abs/2403.16989 (2024).
7. Dai, L. & Miralda-Escudé, J. Gravitational lensing signatures of axion dark matter minihalos in highly magnified stars. *Astron. J.* **159**, 49 (2020).
8. Dai, L., Venumadhav, T., Kaurov, A. A. & Miralda-Escude, J. Probing dark matter subhalos in galaxy clusters using highly magnified stars. *Astrophys. J.* **867**, 24 (2018).
9. Dai, L. et al. Asymmetric surface brightness structure of caustic crossing arc in SDSS J1226+2152: a case for dark matter substructure. *Mon. Not. R. Astron. Soc.* **495**, 3192–3208 (2020).
10. Abe, K. T., Kawai, H. & Oguri, M. Analytic approach to astrometric perturbations of critical curves by substructures. *Phys. Rev. D* **109**, 083517 (2024).
11. Williams, L. L. R. et al. Flashlights: properties of highly magnified images near cluster critical curves in the presence of dark matter subhalos. *Astrophys. J.* **961**, 200 (2024).
12. Han, X. & Dai, L. Under Einstein's microscope: measuring properties of individual rotating massive stars from extragalactic microcaustic crossings. *Astrophys. J.* **964**, 160 (2024).
13. Windhorst, R. A. et al. On the observability of individual population III stars and their stellar-mass black hole accretion disks through cluster caustic transits. *Astrophys. J. Suppl. Ser.* **234**, 41 (2018).
14. Schauer, A. T. P., Bromm, V., Drory, N. & Boylan-Kolchin, M. On the probability of the extremely lensed z=6.2 Earendel source being a population III star. *Astrophys. J. Lett.* **934**, L6 (2022).
15. Zackrisson, E. et al. The detection and characterization of highly magnified stars with JWST: prospects of finding population III. *Mon. Not. R. Astron. Soc.* **533**, 2727–2746 (2024).
16. Rodney, S. A. et al. Two peculiar fast transients in a strongly lensed host galaxy. *Nat. Astron.* **2**, 324–333 (2018).
17. Kaurov, A. A., Dai, L., Venumadhav, T., Miralda-Escudé, J. & Frye, B. Highly magnified stars in lensing clusters: new evidence in a galaxy lensed by MACS J0416.1-2403. *Astrophys. J.* **880**, 58 (2019).
18. Kelly, P. L. et al. Constraints on the Hubble constant from supernova Refsdal's reappearance. *Science* **380**, abh1322 (2023).
19. Diego, J. M. et al. JWST's PEARLS: Mothra, a new kaiju star at z=2.091 extremely magnified by MACS0416, and implications for dark matter models. *Astron. Astrophys.* **679**, A31 (2023).
20. Welch, B. et al. A highly magnified star at redshift 6.2. *Nature* **603**, 815–818 (2022).
21. Stetson, P. B. et al. DAOPHOT: a computer program for crowded-field stellar photometry. *Publ. Astron. Soc. Pac.* **99**, 191 (1987).
22. Bertin, E. & Arnouts, S. SExtractor: software for source extraction. *Astron. Astrophys. Suppl. Ser.* **117**, 393–404 (1996).
23. DeCoursey, C. et al. The JADES transient survey: discovery and classification of supernovae in the JADES deep field. Preprint at arxiv.org/abs/2406.05060 (2024).
24. Lejeune, T., Cuisinier, F. & Buser, R. Standard stellar library for evolutionary synthesis. I. Calibration of theoretical spectra. *Astron. Astrophys. Suppl. Ser.* **125**, 229–246 (1997).
25. Rieke, M. J. et al. Performance of NIRCam on JWST in flight. *Publ. Astron. Soc. Pac.* **135**, 028001 (2023).
26. Willott, C. J. et al. The near-infrared imager and slitless spectrograph for the James Webb Space Telescope. II. Wide field slitless spectroscopy. *Publ. Astron. Soc. Pac.* **134**, 025002 (2022).
27. Soucail, G., Fort, B., Mellier, Y. & Picat, J. P. A blue ring-like structure in the center of the A 370 cluster of galaxies. *Astron. Astrophys.* **172**, L14–L16 (1987).

28. Soucail, G., Mellier, Y., Fort, B., Hammer, F. & Mathez, G. Further data on the blue ring-like structure in A 370. *Astron. Astrophys.* **184**, L7–L9 (1987).
29. Lynds, R. & Petrosian, V. Luminous arcs in clusters of galaxies. *Astrophys. J.* **336**, 1–8 (1989).
30. Bushouse, H. et al. *JWST Calibration Pipeline* (STScI, 2023).
31. Rigby, J. et al. The science performance of JWST as characterized in commissioning. *Publ. Astron. Soc. Pac.* **135**, 048001 (2023).
32. Rieke, M. J. et al. JADES initial data release for the Hubble ultra deep field: revealing the faint infrared sky with deep JWST NIRCam imaging. *Astrophys. J. Suppl. Ser.* **269**, 16 (2023).
33. Steinhardt, C. L. et al. The BUFFALO HST Survey. *Astrophys. J. Suppl. Ser.* **247**, 64 (2020).
34. Dey, A. et al. Overview of the DESI Legacy Imaging Surveys. *Astron. J.* **157**, 168 (2019).
35. Gaia Collaboration. et al. Gaia Data Release 2. Summary of the contents and survey properties. *Astron. Astrophys.* **616**, A1 (2018).
36. Perrin, M. D. et al. Updated point spread function simulations for JWST with WebbPSF. In *Proc. SPIE Conference Series, Space Telescopes and Instrumentation 2014: Optical, Infrared, and Millimeter Wave* Vol. 9143 (eds Oschmann, J. et al.) 91433X (SPIE, 2014).
37. Boucaud, A. et al. Convolution kernels for multi-wavelength imaging. *Astron. Astrophys.* **596**, A63 (2016).
38. Virtanen, P. et al. SciPy 1.0: fundamental algorithms for scientific computing in Python. *Nat. Methods* **17**, 261–272 (2020).
39. Dai, L. Statistical microlensing towards magnified high-redshift star clusters. *Mon. Not. R. Astron. Soc.* **501**, 5538–5553 (2021).
40. Mao, S. Introduction to gravitational microlensing. Preprint at arxiv.org/abs/0811.0441 (2008).
41. Harris, W. E. Globular cluster systems in giant ellipticals: the mass/metallicity relation. *Astrophys. J.* **699**, 254–280 (2009).
42. Harris, W. E., Harris, G. L. H. & Alessi, M. A catalog of globular cluster systems: what determines the size of a galaxy's globular cluster population? *Astrophys. J.* **772**, 82 (2013).
43. Kelly, P. L. et al. Flashlights: more than a dozen high-significance microlensing events of extremely magnified stars in galaxies at redshifts $z = 0.7–1.5$. Preprint at arxiv.org/abs/2211.02670 (2022).
44. Diego, J. M. et al. JWST's PEARLS: A new lens model for ACT-CL J0102−4915, 'El Gordo,' and the first red supergiant star at cosmological distances discovered by JWST. *Astron. Astrophys.* **672**, A3 (2023).
45. Meneghetti, M. et al. The Frontier Fields lens modelling comparison project. *Mon. Not. R. Astron. Soc.* **472**, 3177–3216 (2017).
46. Tuntsov, A. V., Lewis, G. F., Ibata, R. A. & Kneib, J. P. Detecting compact dark matter in galaxy clusters via gravitational microlensing: A2218 and A370. *Mon. Not. R. Astron. Soc.* **353**, 853–866 (2004).
47. Diego, J. M. et al. Imaging dark matter at the smallest scales with $z \approx 1$ lensed stars. *Astron. Astrophys.* **689**, A167 (2024).
48. Rawle, T. D. et al. A complete census of Herschel-detected infrared sources within the HST Frontier Fields. *Mon. Not. R. Astron. Soc.* **459**, 1626–1645 (2016).
49. Patrício, V. et al. Kinematics, turbulence, and star formation of $z \sim 1$ strongly lensed galaxies seen with MUSE. *Mon. Not. R. Astron. Soc.* **477**, 18–44 (2018).
50. Graham, M. L. et al. The type II supernova rate in $z \sim 0.1$ galaxy clusters from the Multi-Epoch Nearby Cluster Survey. *Astrophys. J.* **753**, 68 (2012).
51. Golubchik, M. et al. A search for transients in the Reionization Lensing Cluster Survey (RELICS): three new supernovae. *Mon. Not. R. Astron. Soc.* **522**, 4718–4727 (2023).
52. Graur, O. et al. A year-long plateau in the late-time near-infrared light curves of type Ia supernovae. *Nat. Astron.* **4**, 188–195 (2020).
53. Kwok, L. A. et al. A JWST near- and mid-infrared nebular spectrum of the type Ia supernova 2021aefx. *Astrophys. J. Lett.* **944**, L3 (2023).
54. Abbott, B. P. et al. Multi-messenger observations of a binary neutron star merger. *Astrophys. J. Lett.* **848**, L12 (2017).
55. Villar, V. A. et al. The combined ultraviolet, optical, and near-infrared light curves of the kilonova associated with the binary neutron star merger GW170817: unified data set, analytic models, and physical implications. *Astrophys. J. Lett.* **851**, L21 (2017).
56. Kawaguchi, K., Shibata, M. & Tanaka, M. Diversity of kilonova light curves. *Astrophys. J.* **889**, 171 (2020).
57. Smith, N. et al. Massive star mergers and the recent transient in NGC 4490: a more massive cousin of V838 Mon and V1309 Sco. *Mon. Not. R. Astron. Soc.* **458**, 950–962 (2016).
58. Oguri, M. The mass distribution of SDSS J1004+4112 revisited. *Publ. Astron. Soc. Jpn* **62**, 1017 (2010).
59. Kawamata, R. et al. Size-luminosity relations and UV luminosity functions at $z = 6–9$ simultaneously derived from the complete Hubble Frontier Fields data. *Astrophys. J.* **855**, 4 (2018).
60. Hsiao, E. Y. et al. K-corrections and spectral templates of type Ia supernovae. *Astrophys. J.* **663**, 1187–1200 (2007).
61. Barbary, K. et al. SNCosmo. *Zenodo* https://doi.org/10.5281/zenodo.10684802 (2024).
62. Matharu, J. The Canadian NIRISS Unbiased Cluster Survey (CANUCS). *MAST* https://doi.org/10.17909/ph4n-6n76 (2023).
63. Diego, J. M., Tegmark, M., Protopapas, P. & Sandvik, H. B. Combined reconstruction of weak and strong lensing data with WSLAP. *Mon. Not. R. Astron. Soc.* **375**, 958–970 (2007).
64. Diego, J. M. et al. A free-form lensing model of A370 revealing stellar mass dominated BCGs, in Hubble Frontier Fields images. *Mon. Not. R. Astron. Soc.* **473**, 4279–4296 (2018).
65. Jullo, E. & Kneib, J. P. Multiscale cluster lens mass mapping. I. Strong lensing modelling. *Mon. Not. R. Astron. Soc.* **395**, 1319–1332 (2009).
66. Niemiec, A. et al. Beyond the ultradeep frontier fields and legacy observations (BUFFALO): a high-resolution strong+weak-lensing view of Abell 370. *Mon. Not. R. Astron. Soc.* **524**, 2883–2910 (2023).
67. Zitrin, A. et al. New multiply-lensed galaxies identified in ACS/NIC3 observations of Cl0024+1654 using an improved mass model. *Mon. Not. R. Astron. Soc.* **396**, 1985–2002 (2009).
68. Madore, B. F., Freedman, W. L., Lee, A. J. & Owens, K. Milky Way zero-point calibration of the JAGB method: using thermally pulsing AGB stars in galactic open clusters. *Astrophys. J.* **938**, 125 (2022).

Acknowledgements

We thank L. Kwok for kindly sharing the JWST spectrum of supernova 2021aefx and J. Miralda-Escude for insightful comments. This work is based on observations made with the NASA/ESA/CSA JWST. The data were obtained from the Mikulski Archive for Space Telescopes at the Space Telescope Science Institute, which is operated by the Association of Universities for Research in Astronomy, Inc., under NASA Contract No. NAS5-03127 for JWST. These observations are associated with Programmes 1208 and 3538. We acknowledge the JWST GO-3538 team led by PI E. Iani for developing their observing programme with a zero-exclusive-access period. This work was supported by JSPS (KAKENHI Grant Nos. JP22K21349, JP23K13149, JP20H05856, JP22H01260 and JP22J21). F.S., E.E. and Y.Z. acknowledge the JWST/NIRCam contract to the University of Arizona (Contract No. NAS5-02015). F.S. acknowledges support for Programme 2883 provided by NASA through a grant from the Space Telescope Science Institute. J.M.D. acknowledges support from

the Ministerio de Ciencia, Investigación y Universidades (Project PID2022-138896NB-C51 through MCIU/AEI/MINECO/FEDER, UE). L.D. acknowledges research grant support from the Alfred P. Sloan Foundation (Award Number FG-2021-16495) and the support of the Frank and Karen Dabby STEM Fund in the Society of Hellman Fellows. A.Z. acknowledges support from the United States–Israel Binational Science Foundation (Grant No. 2020750), the United States National Science Foundation (NSF; Grant No. 2109066), the Ministry of Science & Technology, Israel, and the Israel Science Foundation (Grant No. 864/23). E.Z. acknowledges Project Grant No. 2022-03804 from the Swedish Research Council (Vetenskapsrådet) and has also benefited from a sabbatical at the Swedish Collegium for Advanced Study. M.J. is supported by the United Kingdom Research and Innovation (UKRI) Future Leaders Fellowship 'Using Cosmic Beasts to uncover the Nature of Dark Matter' (Grant Nos. MR/S017216/1 and MR/X006069/1). D.J.L. acknowledges support from the UKRI FLF (Grant Nos. MR/S017216/1 and MR/X006069/1). D.J.L. is also supported by Science and Technology Facilities Council (Grant Nos. ST/T000244/1 and ST/W002612/1). E.I. acknowledges funding from the Netherlands Research School for Astronomy (NOVA). R.A.W. and S.H.C. acknowledge support from the NASA JWST Interdisciplinary Scientist programme (Grant Nos. NAG5-12460, NNX14AN10G and 80NSSC18K0200 from GSFC). C.-C.C. acknowledges support from the National Science and Technology Council of Taiwan (Grant No. 111-2112M-001-045-MY3) and Academia Sinica through a Career Development Award (AS-CDA-112-M02). D.E. acknowledges support from a Beatriz Galindo senior fellowship (BG20/00224) from the Spanish Ministry of Science and Innovation and from Projects PID2020-114414GB-100 and PID2020-113689GB-I00 financed by MCIN/AEI/10.13039/501100011033, Project P20-00334 financed by the Junta de Andalucía and Project A-FQM-510-UGR20 of the FEDER/Junta de Andalucía-Consejería de Transformación Económica, Industria, Conocimiento y, Universidades. K.K. acknowledges support from the JSPS (KAKENHI Grant Nos. JP17H06130, JP22H04939, JP23K20035 and JP24H00004). G.E.M. acknowledges financial support from Villum Young Investigator Grant Nos 37440 and 13160 and the Cosmic Dawn Center (DAWN), which is funded by the Danish National Research Foundation (Grant No. 140). A. Nabizadeh acknowledges funding from Olle Engkvists Stiftelse. F.E.B. acknowledges support from ANID-Chile BASAL CATA (Grant No. FB210003), FONDECYT Regular (Grant No. 1241005) and the Millennium Science Initiative (Programmes AIM23-0001 and ICN12_009). P.L.K. acknowledges Grant No. AAG 2308051 from the NSF.

Author contributions

Y.F. wrote the main part of the text, analysed the data and produced the figures. F.S. calibrated and analysed the data and contributed text. J.M.D., M.O., A.Z., M.J., D.J.L., A.M.K. and H.K. contributed analyses and interpretations of the results. E.Z. contributed SED fitting of detected stars. E.E. and R.A.W. contributed interpretations of the data. E.I. contributed to the planning and execution of the JWST GO-3538 programmes. All co-authors contributed to the scientific interpretation of the results and helped to write the manuscript.

Competing interests

The authors declare no competing interests.

Additional information

Supplementary information The online version contains supplementary material available at https://doi.org/10.1038/s41550-024-02432-3.

Correspondence and requests for materials should be addressed to Yoshinobu Fudamoto.

Peer review information *Nature Astronomy* thanks the anonymous reviewers for their contribution to the peer review of this work.

Reprints and permissions information is available at www.nature.com/reprints.

Publisher's note Springer Nature remains neutral with regard to jurisdictional claims in published maps and institutional affiliations.

Springer Nature or its licensor (e.g. a society or other partner) holds exclusive rights to this article under a publishing agreement with the author(s) or other rightsholder(s); author self-archiving of the accepted manuscript version of this article is solely governed by the terms of such publishing agreement and applicable law.

© The Author(s), under exclusive licence to Springer Nature Limited 2025

Yoshinobu Fudamoto[1,2] ✉, Fengwu Sun[2,3], Jose M. Diego[4], Liang Dai[5], Masamune Oguri[1,6], Adi Zitrin[7], Erik Zackrisson[8,9], Mathilde Jauzac[10,11,12,13], David J. Lagattuta[10,11], Eiichi Egami[2], Edoardo Iani[14], Rogier A. Windhorst[15], Katsuya T. Abe[1], Franz Erik Bauer[16,17,18], Fuyan Bian[19], Rachana Bhatawdekar[20], Thomas J. Broadhurst[21,22,23], Zheng Cai[24], Chian-Chou Chen[25], Wenlei Chen[26], Seth H. Cohen[15], Christopher J. Conselice[27], Daniel Espada[28,29], Nicholas Foo[15], Brenda L. Frye[30], Seiji Fujimoto[31], Lukas J. Furtak[7], Miriam Golubchik[7], Tiger Yu-Yang Hsiao[32], Jean-Baptiste Jolly[33], Hiroki Kawai[34], Patrick L. Kelly[35], Anton M. Koekemoer[1,36], Kotaro Kohno[37,38], Vasily Kokorev[14], Mingyu Li[24], Zihao Li[24], Xiaojing Lin[2,24], Georgios E. Magdis[39,40,41], Ashish K. Meena[7], Anna Niemiec[10,11,42], Armin Nabizadeh[8], Johan Richard[43], Charles L. Steinhardt[41,44], Yunjing Wu[24], Yongda Zhu[2] & Siwei Zou[24,45]

[1]Center for Frontier Science, Chiba University, Chiba, Japan. [2]Steward Observatory, University of Arizona, Tucson, AZ, USA. [3]Center for Astrophysics, Harvard & Smithsonian, Cambridge, MA, USA. [4]Instituto de Física de Cantabria (CSIC-UC), Santander, Spain. [5]Department of Physics, University of California, Berkeley, Berkeley, CA, USA. [6]Department of Physics, Graduate School of Science, Chiba University, Chiba, Japan. [7]Department of Physics, Ben-Gurion University of the Negev, Be'er-Sheva, Israel. [8]Observational Astrophysics, Department of Physics and Astronomy, Uppsala University, Uppsala, Sweden. [9]Swedish Collegium for Advanced Study, Uppsala, Sweden. [10]Centre for Extragalactic Astronomy, Durham University, Durham, UK. [11]Institute for Computational Cosmology, Durham University, Durham, UK. [12]Astrophysics Research Centre, University of KwaZulu-Natal, Durban, South Africa. [13]School of Mathematics, Statistics & Computer Science, University of KwaZulu-Natal, Durban, South Africa. [14]Kapteyn Astronomical Institute, University of Groningen, Groningen, The Netherlands. [15]School of Earth and Space Exploration, Arizona State University, Tempe, AZ, USA. [16]Instituto de Astrofísica and Centro de Astroingeniería, Facultad de Física, Pontificia Universidad Católica de Chile, Campus San Joaquín, Macul Santiago, Chile. [17]Millennium Institute of Astrophysics, Providencia, Chile. [18]Space Science Institute, Boulder, CO, USA. [19]European Southern Observatory,

Vitacura, Chile. [20]European Space Agency (ESA), European Space Astronomy Centre (ESAC), Madrid, Spain. [21]Department of Physics, University of the Basque Country, Bilbao, Spain. [22]Donostia International Physics Centre, San Sebastian, Spain. [23]Ikerbasque, Basque Foundation for Science, Bilbao, Spain. [24]Department of Astronomy, Tsinghua University, Beijing, China. [25]Academia Sinica Institute of Astronomy and Astrophysics (ASIAA), Taipei, Taiwan. [26]Department of Physics, Oklahoma State University, Stillwater, OK, USA. [27]Jodrell Bank Centre for Astrophysics, University of Manchester, Manchester, UK. [28]Departamento de Física Teórica y del Cosmos, Universidad de Granada, Granada, Spain. [29]Instituto Carlos I de Física Teórica y Computacional, Facultad de Ciencias, Granada, Spain. [30]Department of Astronomy/Steward Observatory, University of Arizona, Tucson, AZ, USA. [31]Department of Astronomy, University of Texas at Austin, Austin, TX, USA. [32]Center for Astrophysical Sciences, Department of Physics and Astronomy, Johns Hopkins University, Baltimore, MD, USA. [33]Max-Planck-Institut für Extraterrestrische Physik (MPE), Garching, Germany. [34]Department of Physics, University of Tokyo, Tokyo, Japan. [35]Minnesota Institute for Astrophysics, University of Minnesota, Minneapolis, MN, USA. [36]Space Telescope Science Institute, Baltimore, MD, USA. [37]Institute of Astronomy, Graduate School of Science, University of Tokyo, Mitaka, Japan. [38]Research Center for the Early Universe, Graduate School of Science, University of Tokyo, Tokyo, Japan. [39]Cosmic Dawn Center (DAWN), Lyngby, Denmark. [40]DTU-Space, Technical University of Denmark, Kongens Lyngby, Denmark. [41]Niels Bohr Institute, University of Copenhagen, Copenhagen, Denmark. [42]LPNHE, CNRS/IN2P3, Sorbonne Université, Université Paris-Cité, Laboratoire de Physique Nucléaire et de Hautes Énergies, Paris, France. [43]Univ Lyon, Univ Lyon1, Ens de Lyon, CNRS, Centre de Recherche Astrophysique de Lyon, Saint-Genis-Laval, France. [44]Dark Cosmology Centre, Niels Bohr Institute, University of Copenhagen, Copenhagen, Denmark. [45]Chinese Academy of Sciences, South America Center for Astronomy, National Astronomical Observatories, CAS, Beijing, China.
✉e-mail: yoshinobu.fudamoto@gmail.com